iScience

CellPress
OPEN ACCESS

Article

Noninvasive neuromodulation protects against doxorubicin-induced cardiotoxicity and inhibits tumor growth

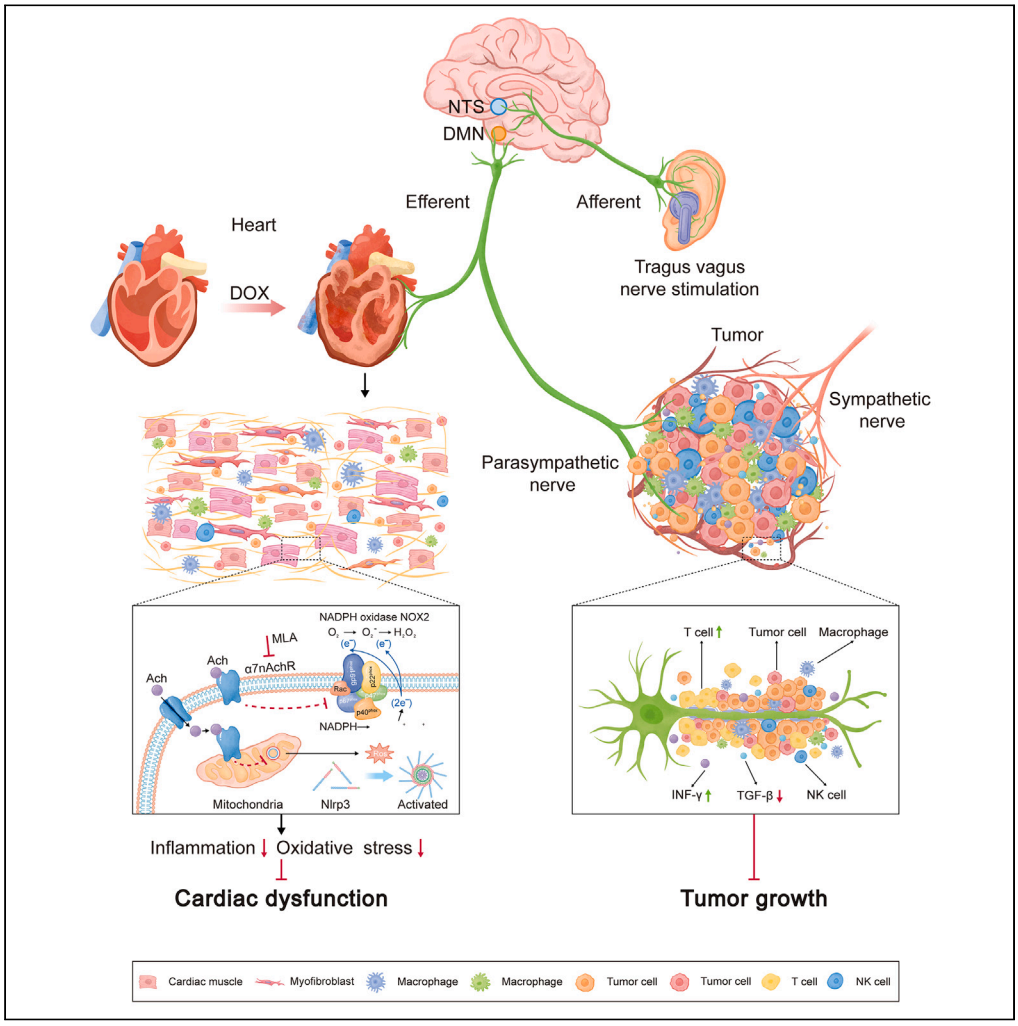

Mengjie Xie, Fuding Guo, Lingpeng Song, ..., Xiaoya Zhou, Hong Jiang, Lilei Yu

whuzhouxiaoya@whu.edu.cn (X.Z.)
hong-jiang@whu.edu.cn (H.J.)
lileiyu@whu.edu.cn (L.Y.)

Highlights

The tVNS plays a dual role in preventing cardiotoxicity and suppressing tumor growth

These effects are mediated through the α7nAchR pathway

Inflammatory response and NADPH oxidase activity are the potential mechanisms

This study provides a promising candidate for cardiovascular and cancer patients

Xie et al., iScience 27, 109163
March 15, 2024
https://doi.org/10.1016/j.isci.2024.109163

iScience

CellPress
OPEN ACCESS

Article

Noninvasive neuromodulation protects against doxorubicin-induced cardiotoxicity and inhibits tumor growth

Mengjie Xie,[1,2] Fuding Guo,[1,2] Lingpeng Song,[1,2] Wuping Tan,[1] Xinrui Han,[1] Saiting Xu,[1] Xujun Li,[1] Yijun Wang,[1] Yueyi Wang,[1] Liping Zhou,[1] Xiaoya Zhou,[1,*] Hong Jiang,[1,*] and Lilei Yu[1,3,*]

SUMMARY

Doxorubicin (Dox) poses a considerable threat to patients owing to its cardiotoxicity, thus limiting its clinical utility. Optimal cardioprotective intervention strategies are needed to suppress tumor growth but also minimize cardiac side effects. Here, we showed that tragus vagus nerve stimulation (tVNS) improved the imbalanced autonomic tone, ameliorated impaired cardiac function and fibrosis, attenuated myocyte apoptosis, and mitochondrial dysfunction compared to those in the Dox group. The beneficial effects were attenuated by methyllycaconitine citrate (MLA). The transcript profile revealed that there were 312 differentially expressed genes and the protection of tVNS and retardation of MLA were related to inflammatory response and NADPH oxidase activity. In addition, tVNS synergizing with Dox inhibited tumor growth and lung metastasis and promoted apoptosis of tumor cells in an anti-tumor immunity manner. These results indicated that non-invasive neuromodulation can play a dual role in preventing Dox-induced cardiotoxicity and suppressing tumor growth through inflammation and oxidative stress.

INTRODUCTION

Doxorubicin (Dox) is a highly effective antitumor agent that is utilized for treating solid tumors such as breast cancer, while hampered its clinical use by cardiotoxicity, inducing inflammation, apoptosis, and oxidative stress, leading to irreversible cardiomyocyte damage and ultimately heart failure.[1,2] Although the early clinical evaluation of cardiotoxicity has been used to manage cardiotoxicity associated with chemotherapy, the efficacy of commonly used cardioprotective agents in clinical practice remains cryptic.[3] Optimal cardioprotective intervention strategies are essential and can play a dual function in minimizing cardiac side effects and anti-tumor effects. Previous studies have revealed that the disturbance of autonomic activity to the heart is regarded to be one of the key contributing factors in the pathophysiologic process of Dox-induced cardiotoxicity.[4] Prior to left ventricular (LV) dysfunction, patients treated with anthracyclines present increased cardiac sympathetic activity.[5] Preclinical and clinical studies have demonstrated that restoring the balance of autonomic tone could improve myocardial inflammation and oxidative stress and therefore reverse the LV dysfunction induced by Dox.[4,6] Furthermore, autonomic nervous system dysfunction is common in breast cancer patients.[7] Clinical studies have indicated that increased sympathetic and decreased vagus nerve density in several tumors is associated with poor long-term survival.[8] Herein, we hypothesized that the modulation of the autonomic nervous system holds the potential for achieving a dual protective effect on both the cardiovascular system and tumorigenesis.

Tragus vagus nerve stimulation (tVNS), as a non-invasive autonomic neuromodulation strategy, exerts prominent anti-inflammation, metabolic remodeling, and mitochondrial protective effects in heart failure modes,[9,10] as well as in myocardial ischemia-reperfusion injury and arrhythmia.[11,12] Importantly, our recent study showed that vagus nerve stimulation ameliorated Dox-induced cardiac dysfunction, but the underlying mechanism has not been elucidated.[4] Vagus nerve stimulation acts on alpha7 nicotinic acetylcholine receptor (α7nAChR) to inhibit pro-inflammatory cytokines in multiple inflammatory diseases.[13,14] In particular, α7nAChR can influence other types of cells *in vivo* and play a crucial role in mitochondrial oxidative stress to cardiomyocytes.[15] The co-administration of varenicline, an α7nAChR agonist, and Dox was found to enhance survival outcomes relative to treatment with Dox alone.[16] In this study, we hypothesized that the anti-inflammatory and mitochondrial protective effects of tVNS are mediated through an α7nAChR-dependent pathway, underlie the amelioration of Dox-induced cardiotoxicity and fibrosis. Therefore, we investigated the effects of tVNS on Dox-induced cardiac dysfunction, inflammation, and oxidative stress in the presence of α7nAChR pharmacological blockade in a mouse breast cancer model and, more importantly, explored its effects on tumor growth and metastasis.

[1]Department of Cardiology, Renmin Hospital of Wuhan University; Institute of Molecular Medicine, Renmin Hospital of Wuhan University; Hubei Key Laboratory of Autonomic Nervous System Modulation; Taikang Center for Life and Medical Sciences, Wuhan University; Cardiac Autonomic Nervous System Research Center of Wuhan University; Hubei Key Laboratory of Cardiology; Cardiovascular Research Institute, Wuhan University, Wuhan 430060, P.R. China
[2]These authors contributed equally
[3]Lead contact
*Correspondence: whuzhouxiaoya@whu.edu.cn (X.Z.), hong-jiang@whu.edu.cn (H.J.), lileiyu@whu.edu.cn (L.Y.)
https://doi.org/10.1016/j.isci.2024.109163

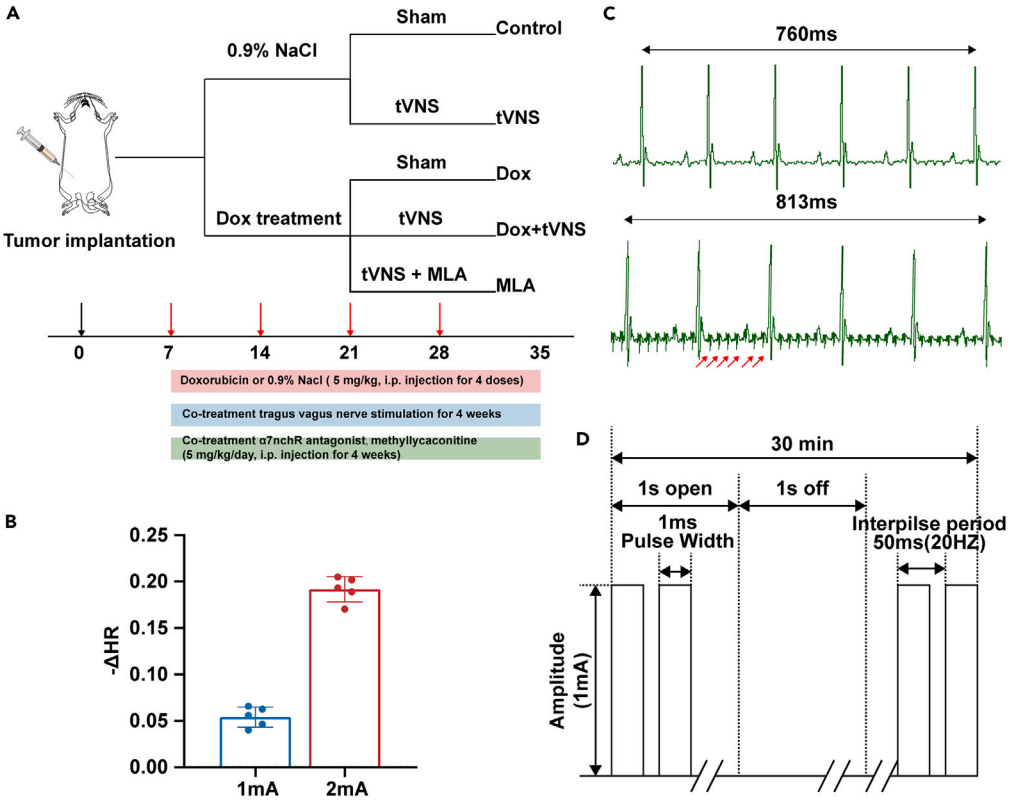

Figure 1. Study protocol and preferences settings for noninvasive transcutaneous vagus nerve stimulation (tVNS)

(A) Schematic of the study design, group assignment, and endpoints.

(B) Changes in heart rate before and during tVNS at baseline at different stimulation intensities (n = 5).

(C) Representative ECG tracings from a mouse at baseline and during active tVNS at 1 mA, indicating a modest prolongation of the RR interval during active stimulation. Arrows indicate the stimulation artifact.

(D) Optimal parameters for tVNS, a 20-HZ frequency and 1 mA amplitude with a pulse width of 1 ms were applied with duty cycles of 1 s on and 1 s off for 30 min per day.

RESULTS

tVNS improves cardiac autonomic function induced by Dox

The animal experimental protocol and parameter chosen were shown in Figure 1. To determine the effectiveness of tVNS on autonomic tone, Heart rate variability (HRV) was evaluated in mice from various groups. Compared to the control group, Dox significantly decreased high frequency (HF) (61.58 ± 4.27 vs. 75.83 ± 2.12 nu., $p < 0.0001$), but increased low frequency (LF) (36.68 ± 3.83 vs. 24.68 ± 2.34 nu., $p < 0.0001$) and LF/HF (0.63 ± 0.11 vs. 0.33 ± 0.04, $p < 0.0001$) (Figures 2A–2C). For the Dox+tVNS group, tVNS prevented these changes induced by Dox and restored to the control group. Additionally, the presence of methyllycaconitine citrate (MLA) reversed this protective effect. As shown in Figures 2D and 2E, a significant decrease ($p < 0.001$) in serum acetylcholine (ACH) and an increase ($p < 0.0001$) in norepinephrine (NE) were observed in the Dox group, while tVNS increased the 84.65% Ach and reduced 17.8% NE level in Dox+tVNS vs. Dox group, suggesting an antiadrenergic effect. Conversely, the MLA-treated mice showed similar circulation ACH ($p = 0.48$) and NE level ($p = 0.78$) to that of the Dox group. Furthermore, following treatment with Dox, which led to parasympathetic denervation, an increase in cardiac tyrosine hydroxylase (TH) sympathetic fibers was observed (Figures 2F and 2G). These results indicated that tVNS could improve the impaired sympathetic overactivity and low vagal tone induced by Dox, whereas this protection was blocked by MLA.

tVNS alleviated Dox-induced cardiac dysfunction and cardiac injury

Echocardiography was conducted after the last Dox administration. LV ejection fraction (LVEF) (68.72 ± 2.95 vs. 54.21 ± 2.87%, $p < 0.0001$) and fractional shortening (FS) (33.48 ± 2.11 vs. 24.44 ± 2.42%, $p < 0.0001$) were significantly improved in the tVNS group compared to those of the Dox group, whereas this effect was reversed by MLA treatment (56.05 ± 3.47% and 25.47 ± 2.50%, respectively) (Figures 3A–3C). Dox treatment resulted in a decline in stroke volume (SV) and an increase in LV internal diameters and tVNS therapy attenuated the internal diameters expansion (supplemental information, Figures S1A–S1C). Conversely, a significant increase in LV internal dimension in systole (LVIDs) and in diastole (LVIDd) and a decrease in SV were detected in the MLA group compared to the Dox+tVNS group. Moreover, the heart

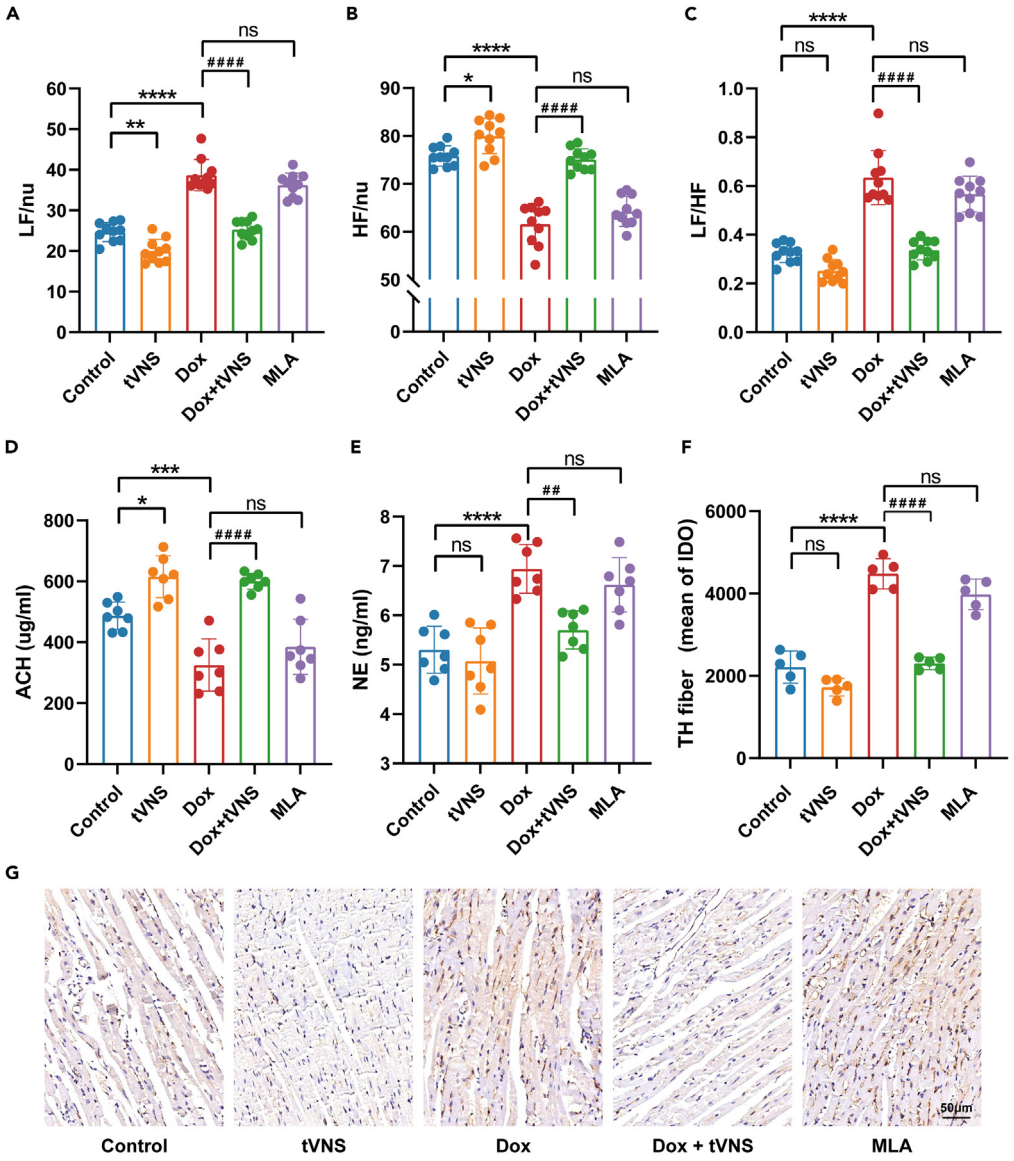

Figure 2. tVNS affected heart rate variability and altered cardiac autonomic nerve fiber innervation

(A–C) Frequency domain analysis using the Fast Fourier Transform method (n = 10). LF, low frequency; HF, high frequency.

(D and E) Serum acetylcholine (ACH) and norepinephrine (NE) in various groups (n = 7).

(F and G) Quantification of TH^+ sympathetic nerve density in the cardiac tissue (n = 5), and the representative image of TH expression assessed by immunohistochemistry. TH, tyrosine hydroxylase; IDO, mean of integral optical density. (*p < 0.05, **p < 0.01, ***p < 0.001, ****p < 0.0001 vs. control group; $^{\#\#}$p < 0.01, $^{\#\#\#\#}$p < 0.0001 vs. Dox group; one-way ANOVA analysis with Tukey's multiple comparisons test was used for statistical analysis. Values represent mean ± SD).

weight (normalized to tibia length) was markedly decreased by 18.3% in the Dox-treated mice, which was mitigated with tVNS therapy (6.55 ± 0.71 vs. 5.40 ± 0.37 mg/mm, p < 0.05) (Figure 3D). The serum creatine kinase MB isoenzyme (CK-MB) and cardiac troponin T (cTnT), and the mRNA expressions of ANP and BNP were also notably increased in Dox groups and were restored to the control levels in mice treated with tVNS (Figures 3E–3G), whereas MLA overtly blocked this effect, suggesting α7nAChR partly mediated the protection for cardiac injury.

tVNS alleviates Dox-induced cardiac myocyte apoptosis and mitochondrial dysfunction

Representative images of Masson's trichrome staining were presented interstitial and perivascular fibrosis induced by Dox, which were stained blue for collagen fibers (Figure 4A). In comparison with the Dox group, the cardiac fibrosis of LV was reduced in the Dox+tVNS group (2.68 ± 0.68% vs. 12.52 ± 1.80%, p < 0.0001), while this effect could be partially blocked by MLA (9.27 ± 1.71%) (Figure 4B). The

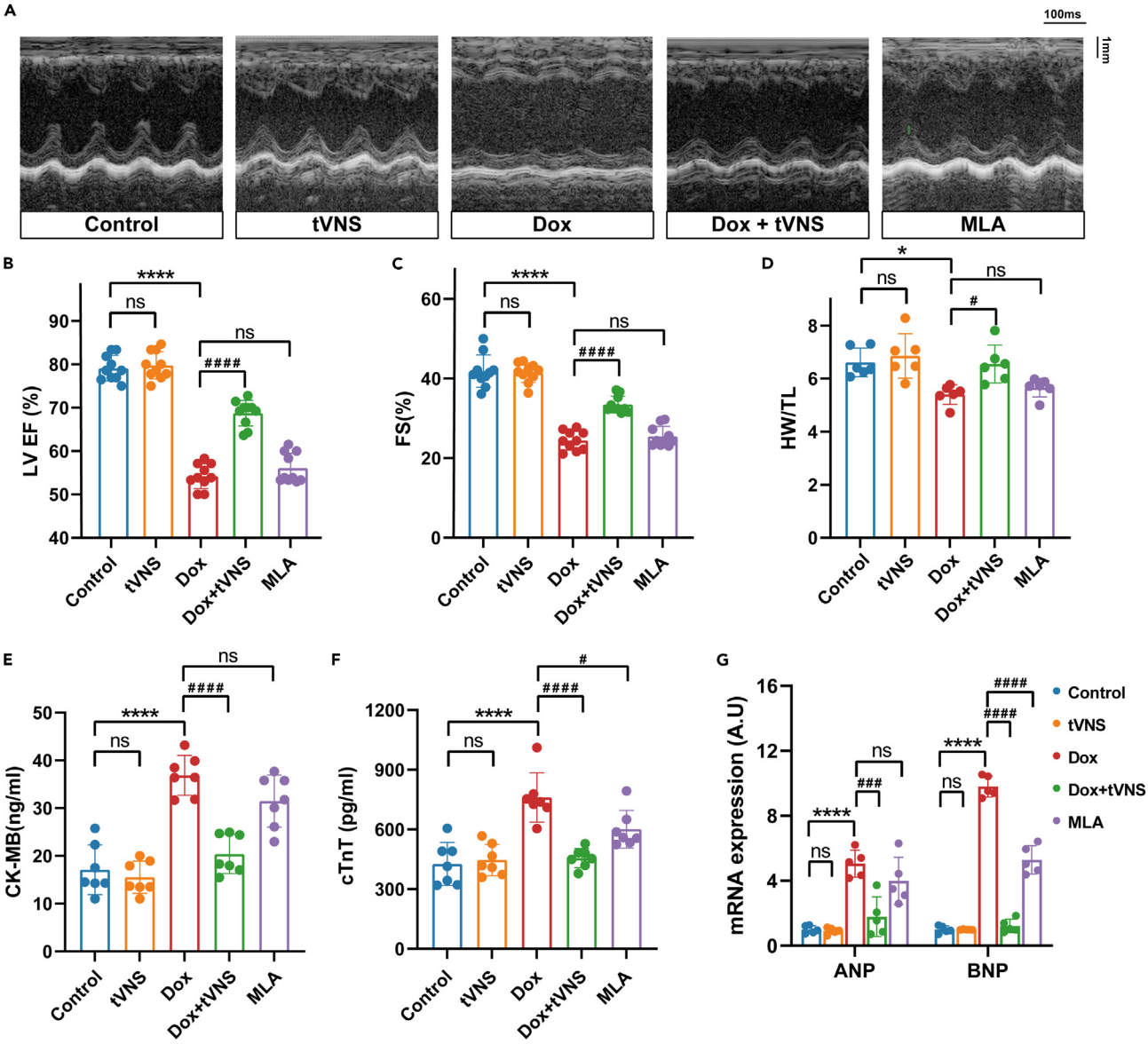

Figure 3. tVNS alleviates Dox-induced cardiac dysfunction

(A) Representative M-mode echocardiographic images from various groups.

(B and C) Echocardiography analysis of the LVEF%, and FS%, respectively (n = 10). LVEF%, left ventricular ejection fraction; FS%, fractional shortening.

(D) Heart weight normalized to tibia length (n = 6).

(E and F) Serum Creatine Kinase MB Isoenzyme (CK-MB) and cardiac troponin T (cTnT) in various group after the last dose of Dox or saline (n = 7).

(G) Relative mRNA expressions of ANP and BNP in cardiac tissues from difference groups (n = 5). (*$p < 0.05$, ****$p < 0.0001$ vs. control group; $^{\#}p < 0.05$, $^{\#\#}p < 0.01$, $^{\#\#\#\#}p < 0.0001$ vs. Dox group; one-way ANOVA analysis with Tukey's multiple comparisons test was used for statistical analysis. Values represent mean ± SD).

histopathological examination of heart tissue from different groups revealed that tVNS could significantly improve marked degenerative changes in cardiac fibers and extensive inflammatory infiltration induced by Dox (Figure 4C).

Additionally, Dox increased the number of cardiomyocytes displaying terminal deoxynucleotidyl transferase-mediated dUTP nick and labeling (TUNEL)-positive staining and tVNS could protect myocyte apoptosis (0.94 ± 0.19% vs. 17.63 ± 1.74 vs. 2.95 ± 0.58% in Control, Dox and Dox+tVNS groups, respectively) (Figures 4D and 4E). Given the essential effect of mitochondrial structure on maintaining the normal myocardial function, it was investigated whether tVNS would modulate mitochondrial morphology. In the control and tVNS groups, myocyte myofibrils were arranged in a neat pattern, and mitochondria showed varying shapes and sizes with slight hyperplasia. (Figure 4F). Conversely, the transmission electron microscopy (TEM) images from the mice in the Dox group showed that mitochondria were significantly damaged manifesting moderate swelling, cristae broken and missing, and matrix vacuolated and extravasated. After treatment of tVNS, the impaired

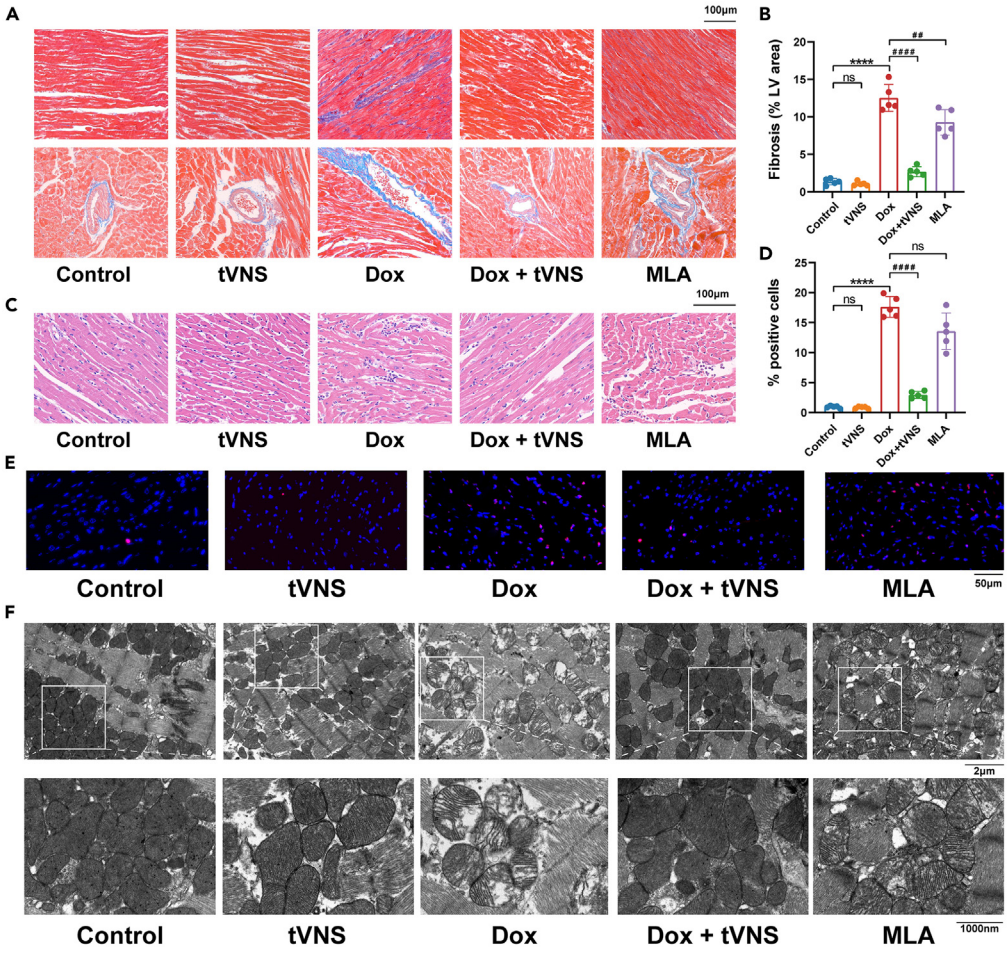

Figure 4. Effect of tVNS on cardiac fibrosis, inflammatory infiltration, and mitochondrial damage

(A) Representative examples of histological images from animals from each group with Masson trichrome showing fibrosis, upper for interstitial fibrosis and lower for vascular fibrosis.

(B) Quantification of fibrosis area (as a percent of the left ventricular area; n = 5).

(C) Representative examples of histological images from animals from each group stained with hematoxylin and eosin.

(D and E) Quantification of TUNEL-positive cells percentage (n = 5) and the representative images of TUNEL staining in different groups.

(F) Transmission electron micrographs of the cardiac tissue, and magnification insets show mitochondrial structure from different groups. (****$p < 0.0001$ vs. control group; $^{\#\#}p < 0.01$, $^{\#\#\#\#}p < 0.0001$ vs. Dox group; one-way ANOVA analysis with Tukey's multiple comparisons test was used for statistical analysis. Values represent mean ± SD).

mitochondrial structure was notably improved. However, this effect was partially blocked by MLA, which was less severe than the effect exerted on the Dox group. These data implicated that Dox could induce cardiac fibrosis, myocyte apoptosis and mitochondrial damage and these effects can be alleviated by tVNS in an α7nAChR-dependent manner.

LV transcriptional profile differs among different groups

To obtain mechanistic insights into differences in phenotype among groups involved in the protective effects of tVNS treatment and blocking effects by MLA, cardiac LV transcriptional profiling was performed in mice of the Dox, Dox+tVNS and MLA groups. As shown in Figures 5A and 5B, genes (relative fold change, ≥1.5; false discovery rate, <0.05) were differentially expressed in the Dox+tVNS group compared with the Dox group, and MLA compared with the Dox+tVNS group, respectively. A total of 312 shared transcripts revealed the part reversed by MLA (Figure 5C). The Kyoto Encyclopedia of Genes and Genomes (KEGG) pathway analysis indicated that these altered genes were primarily referring to the immune system and signaling conduction (Figure 5D). To describe the function of these genes, the Gene Ontology (GO) annotation of molecular function (MF), biological process (BP) and cell component (CC) were further analyzed (Figure 5E). Notably, inflammation-associated gene sets were among the top 10 most significant altered pathway enrichment, including inflammatory response, neutrophil chemotaxis, etc. In the process of CC and MF, nicotinamide adenine dinucleotide phosphate (NADPH) and NAD+ oxidase activity were

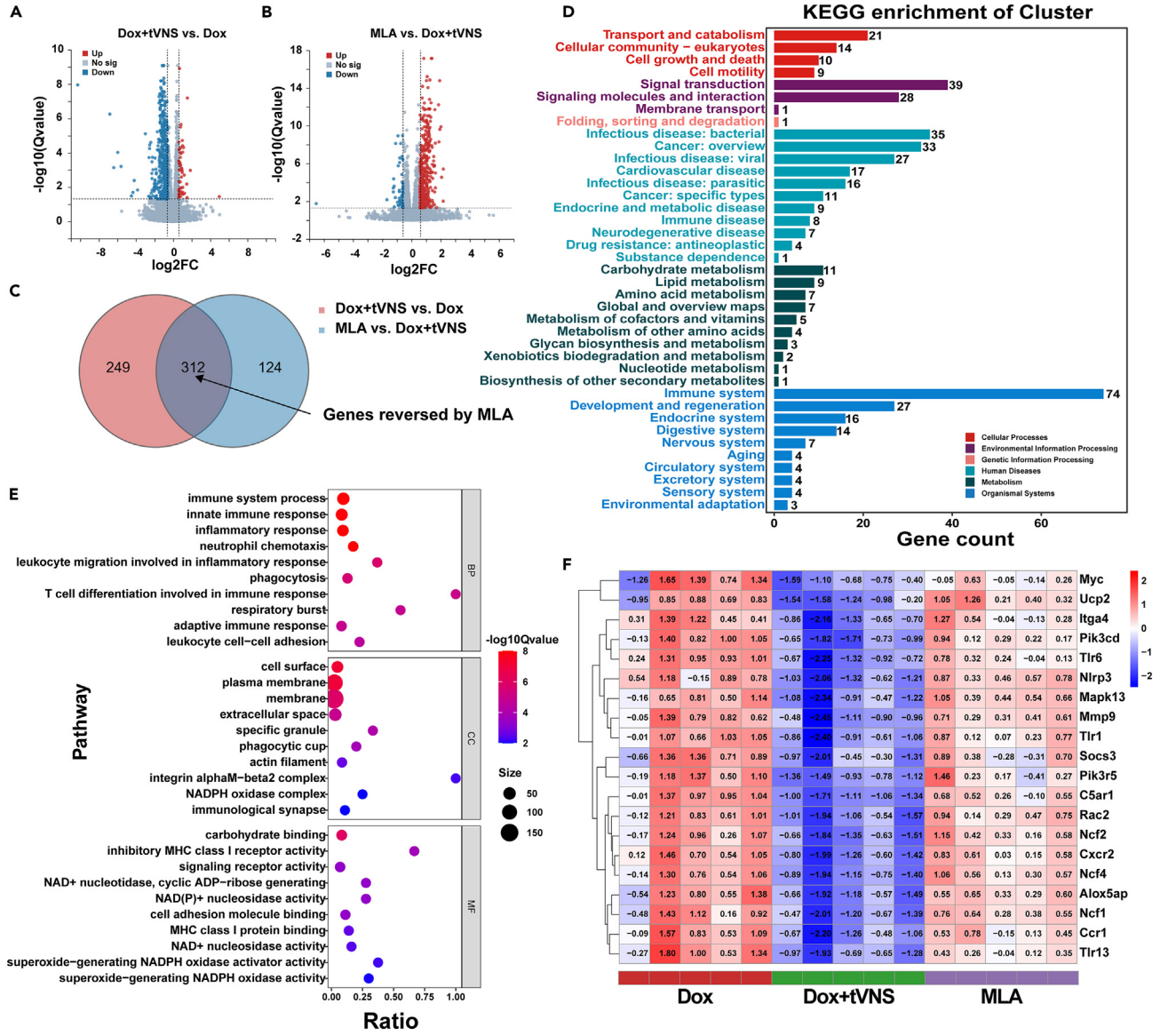

Figure 5. Left ventricular transcriptional profile and functional annotations from various groups

(A and B) Volcano plot presenting differential genes expressing in Dox+tVNS group vs. Dox group, and MLA group vs. Dox+tVNS, respectively.

(C) Venn diagram showing the number of transcripts that were differentially expressed in the Dox group vs. the Dox + tVNS group, and the Dox + tVNS group vs. the MLA group. The shared part represented altered genes reversed by MLA.

(D) Kyoto Encyclopedia of Genes and Genomes (KEGG) classification analysis of the genes (n = 312) that were altered by both tVNS and MLA.

(E) Gene Ontology (GO) pathway analysis of the shared differential genes. BP, biological process; CC, cell component; MF, molecular function.

(F) Heatmap showing the differentially expressed genes in each treatment group.

significantly changed by tVNS and MLA intervention. The heatmap further revealed tVNS nearly normalized the transcriptional profile of what was induced by Dox, whereas the gene expression of the MLA group was intermediate to those between Dox and Dox+tVNS group, suggesting that the MLA treatment caused the partial reversal of the effects of tVNS (Figure 5F). Among all the altered genes, the inflammatory cytokines (Ccr1, Cxcr2, and Nlrp3) and NADPH oxidase 2 (NOX2) subunits encoding genes (Ncf1, NCF2, Ncf4, and Rac2) were focused on in the current study. The mRNA expressions validated by qPCR were coincident with the transcriptional profile used by RNA-seq, which showed that tVNS decreased the elevated expression in the Dox group and MLA reversed these effects (Figures 6A–6G). Compared to Dox group, tVNS significantly downregulated the expression of Ncf1, NCF2, and Rac2, indicating that tVNS treatment also improved cardiac inflammation and oxidations in tumor-bearing mice.

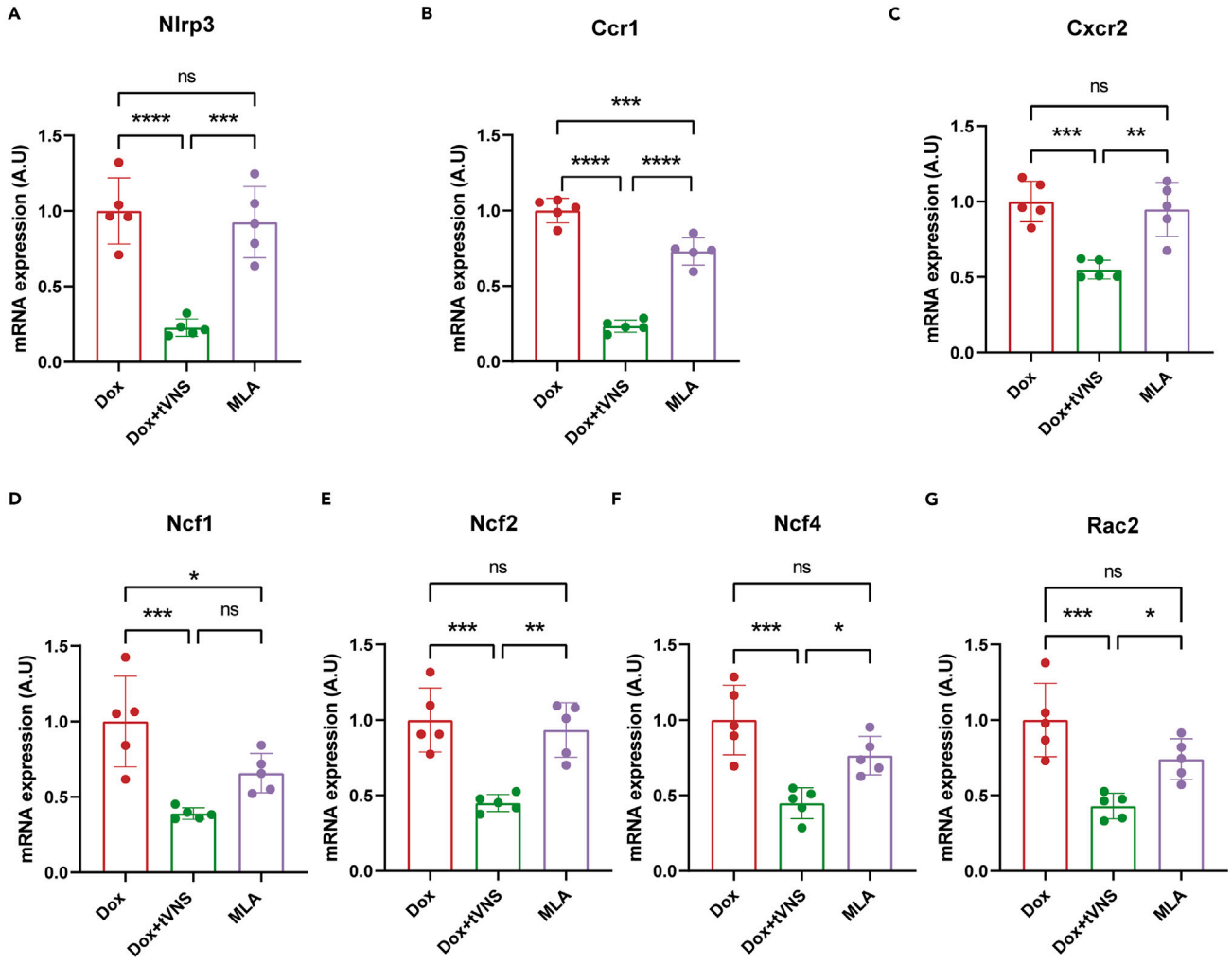

Figure 6. Relative mRNA expressions of key genes involved in inflammation and NADPH oxidase activity

(A–G) Relative mRNA expressions of Ccr1, Cxcr2, Nlrp3, Ncf1, Ncf2, Ncf4, and Rac2 in cardiac tissues from different groups. GAPDH was used for normalization (n = 5). (*p < 0.05, **p < 0.01, ***p < 0.001, ****p < 0.0001 vs. control group; one-way ANOVA analysis with Tukey's multiple comparisons test was used for statistical analysis. Values represent mean ± SD).

tVNS potentiates the anticancer activity of Dox

We further explored whether tVNS could synergize with Dox to exert antitumor effects. Tumor burden was detected in 4T1-luc tumor-bearing BALB/c mice through bioluminescence imaging (BLI) and monitored with a Vernier caliper. Notably, the Dox+tVNS group showed the best tendency in inhibiting tumor growth, and the Dox and MLA groups presented similar antitumor effects (Figures 7A and S2). The BLI signal intensity was correlated with the tumor size but the appearance of tumor necrosis affected the results (Figure 7B). Tumor growth measurement showed slight reduction in tumor volume with no significant difference between the tVNS-treated and control mice ($p > 0.05$) (Figure 7C). However, Dox significantly delayed tumor growth and the combination with tVNS treatment could lead to even smaller tumors, whereas MLA blocked the antitumor effects of the combination therapy (1439.0 ± 135.3 vs. 645.6 ± 78.9 vs. 336.3 ± 105.1 vs. 624.6 ± 150.6 mm^3 in control, Dox, Dox+tVNS and MLA groups, respectively). The mice were sacrificed to evaluate the volumes and weights of excised tumor, which also showed better antitumor activity of the Dox+tVNS combination and were consistent with the previous analysis (Figures 7D and 7E).

Furthermore, As shown in Figure 7F, in the tumor sections of the control group, the tumor cells were tightly packed and diffusely distributed, while various degrees of nuclear shrinkage and fragmentation were observed in other groups. tVNS alone increased tissue necrosis and focal necrosis, which were further reinforced by combination with Dox treatment. This strengthening effect was canceled by the MLA treatment. TUNEL staining in tumor tissues also indicated that the Dox+tVNS treatment caused the most notable apoptosis of tumor cells, while only a few apoptotic cells were found in the control group (Figure 7H). The noticeable inhibition of metastatic foci was also found by the hematoxylin and eosin (H&E) staining of the lungs. Alveolar cavities in Dox+tVNS were more evident than in the Dox group. Meanwhile, the

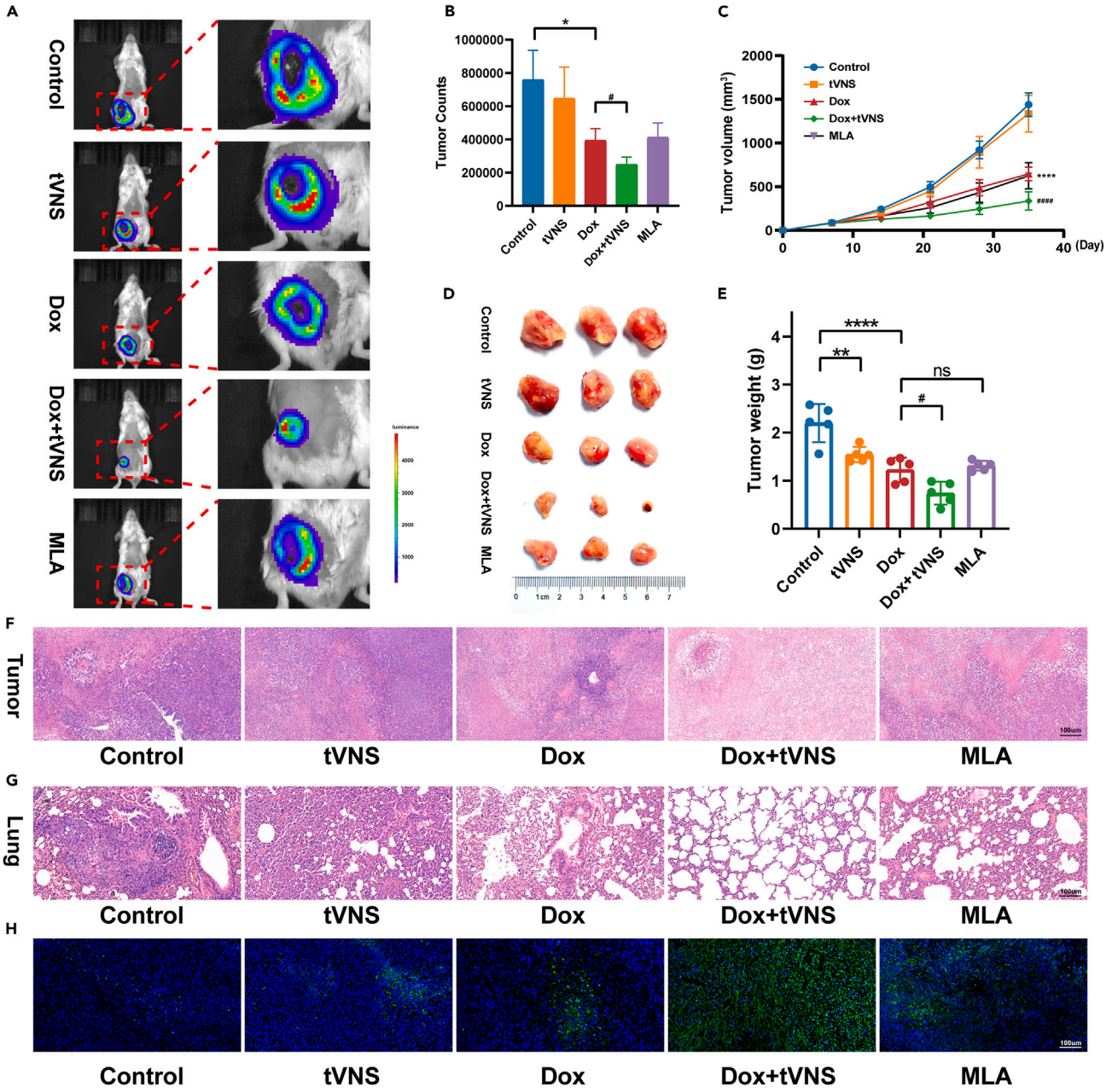

Figure 7. tVNS inhibited the growth and metastasis of tumor

(A) Bioluminescence imaging of primary tumor among groups and (B) were quantified by luciferase intensity (n = 4).

(C) Tumor growth in different groups of mice (n = 9–13).

(D) Representative image of the exfoliated tumor.

(E) Tumor weight was measured to access tumor growth inhibition in various groups (n = 5).

(F) Representative examples of histological images from tumor tissue; the nuclei were stained blue, and the cytoplasm and extracellular matrix were stained pink with hematoxylin and eosin (H&E).

(G) Representative examples of histological images from lung tissue stained with H&E.

(H) Representative images of the TUNEL staining in different groups from tumor tissue. (*$p < 0.05$, ***$p < 0.001$, ****$p < 0.0001$ vs. control group; $^{\#}p < 0.05$, $^{\#\#\#\#}p < 0.0001$ vs. Dox group; one-way ANOVA analysis with Tukey's multiple comparisons test was used for normally distributed statistical analysis. Values represent mean ± SD).

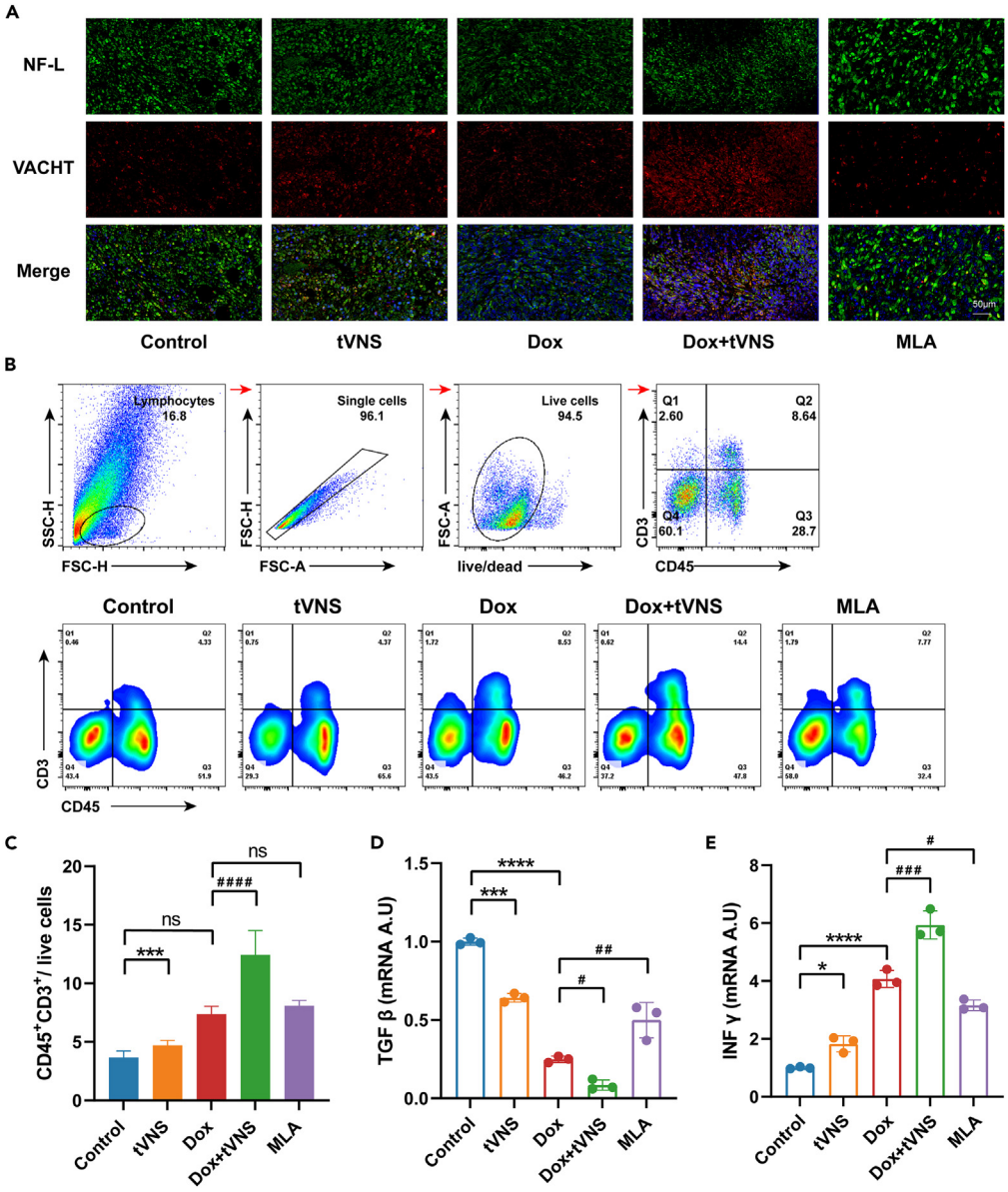

Figure 8. Effects of tVNS on neuromodulation and inflammation in tumor

(A) Neuronal marker NF-L (green) and parasympathetic neuron marker VACHT (red) assessed by immunofluorescence in tumor tissue. NF-L, Neurofilament-L; VACHT, Vesicular acetylcholine transporter.

(B) Flow cytometry sorting protocol and Representative FACS plots.

(C) Relative quantification of $CD45^+CD3^+$ cells (n = 5).

(D and E) relative mRNA expression of TGFβ and INFγ in tumor tissues (n = 3). (*$p < 0.05$, ***$p < 0.001$, ****$p < 0.0001$ vs. control group; $^{\#}p < 0.05$, $^{\#\#}p < 0.01$ and $^{\#\#\#}p < 0.001$, $^{\#\#\#\#}p < 0.0001$ vs. Dox group; one-way ANOVA analysis with Tukey's multiple comparisons test was used for statistical analysis. Values represent mean ± SD).

space-occupying metastatic foci were less and smaller than those in other groups (Figure 7G). And tVNS could further influence the tumor's local autonomic domination (Figure 8A). Despite receiving tVNS intervention, the MLA group showed similar worse tumor invasion and lung metastasis to the Dox group than that in the Dox+tVNS group. Given the synergistic antitumor effect was partly reversed by MLA, tVNS was assumed to be involved in antitumor immunity and therefore, it slowed down tumor progression. The flow cytometry results indicated an increased number of tumor-infiltrating T cells ($CD45^+CD3^+$) in the Dox group (Figures 8B and 8C). In particular, the number of infiltrating T cells in the Dox+tVNS was twice as high as that of the Dox group. Consistently, the Dox treatment led to an increase in IFNγ expression and a decrease in TGFβ expression, while tVNS treatment enhanced this effect, as shown in Figures 8D and 8E. Ultimately, these results indicated that the combination of Dox and tVNS bear the capacity to inhibit tumor progression.

DISCUSSION

In summary, we demonstrated tVNS is an effective strategy for preventing Dox-induced cardiotoxicity. tVNS not only prevented alterations in LV function, but also reduced inflammatory infiltration, cardiac fibrosis, and mitochondrial damage in tumor-bearing mice. Furthermore, the transcript profile revealed that tVNS downregulated the genes associated with inflammation and NADPH oxidative activity. These cardioprotective benefits were inhibited in the presence of pharmacological blockade of the α7nAChR. Further, we identified the anti-tumor effects of tVNS through tumor immune response, which underlies the attenuation in tumor growth and progression. Overall, we provided an insight that tVNS exerted dual benefits on preventing the cardiotoxicity properties of Dox while enhancing its antitumor effect through an α7nAChR-dependent pathway, realizing "killing two birds with one stone" therapy effects.

Dox-associated cardiotoxicity, is a well-known threat to cancer patients, presenting cumulative and dose-dependent.[2] The underlying mechanism is generally involved in inflammation, mitochondrial dysfunction, oxidative stress, DNA damage, and imbalanced cardiac autonomic tone.[17] In our previous study, we demonstrated the potential cardioprotective effects of tVNS, which may be associated with reduced recruitment of pro-inflammatory macrophage and expression of inflammatory chemokine.[4,18] Consistent with the previous study, we found the important role of chemokines and chemokine receptors like CCR1 and CXCR2 in the pathogenesis of Dox-induced cardiotoxicity. In addition, we further found the anti-inflammatory protective effects of tVNS on Dox-induced cardiotoxicity related to innate immunity and its subsequent release of pro-inflammatory cytokines.

Given the fact that anti-inflammatory effects exerted by tVNS are primarily mediated by the cholinergic anti-inflammatory pathway, we hypothesized that these beneficial effects of tVNS on Dox-induced cardiotoxicity were mediated through α7nAChR. As expects, the attenuation of the tVNS effects on cardiac injury, fibrosis, inflammation, apoptosis, and mitochondrial damage was partially blocked by MLA, highlighting a crucial role of α7nAChR in Dox-induced cardiotoxicity, and even heart failure. In this context, we further found that the effect of tVNS is consistent with recent evidence suggesting that an α7nAChR-dependent cholinergic pathway is recruited to improve LV dysfunction. In particular, α7nAChR can influence other types of cells *in vivo* and play a crucial role in mitochondrial oxidative stress to cardiomyocytes.[15]

Our transcripts profiles revealed plasma membrane-localized toll-like receptor 1 (TLR1) and TLR2 were reduced after the treatment of tVNS, where TLR2 forms heterodimers with TLR1 to enable inflammatory responses, and the latter is considerably upregulated in the scar tissue after myocardial infarction and atherosclerosis,[19] involving in cardiac remodeling and fibrosis. As another significant regulatory factor of the innate immune system, Nlrp3 was validated to reduce after the treatment of tVNS. The mRNA expression of Nlrp3 was inversely correlated with the neuroinflammatory response threshold, which subsequently elicit amplified neuroinflammation,[20] thus inducing cascade inflammatory response and pyroptotic cell death.[21] It is likely that ACH could act on the α7nAChR located in the cell surface and mitochondria, modulating the intracellular signaling transduction cascades, downregulating NF-κB-inducing receptors and preventing the release of mtDNA, leading to the prevention of the Nlrp3 inflammasome activation and promoting an anti-inflammatory phenotype.[22,23] These data support that inhibiting of anti-inflammatory effect of tVNS attenuates the antifibrotic effect and underscore the involvement of the innate immune response in Dox-induced cardiotoxicity. Future investigations could further identify chemokines as biomarkers for monitoring Dox-cardiotoxicity and targeting chemokine receptors could be an effective way in reducing leukocytes infiltration into injured hearts and improving cardiac remodeling and dysfunction.

Moreover, our transcriptomic analysis and following validation showed that tVNS participated in the process of NADPH oxidase activity and resulted in a significant decrease in the expression of cytosolic components of NOX2. NOX is a family of multisubunit enzyme complexes that play a crucial role in reactive oxidation species (ROS) generation, which requires binding with subunits to form a stable complex to exert catalysis.[24] The enzymatic complex consists of transmembrane cytochrome *b*558 and cytosolic subunits including, Ncf1, Ncf2, Ncf4, as well as the GTPase Rac1 or Rac2. When cells were stimulated, the physically dissociated subunits instantly migrated to the membrane, leading to exacerbating oxidative stress, activating apoptosis and eventually myocardial injury.[25] Our transcript profiling and qPCR validation showed that tVNS could downregulate the expression of Ncf1, Ncf2, Ncf4, and Rac2. The increase in expression of the regulatory Ncf1 could enhance NOX2-dependent ROS production, and amplified intracellular Ca^{2+} signaling, which latter results in appearance of fibrotic patches, as well as decrease in cardiac contractility.[26–28] Interestingly, the clinical study had demonstrated that the overexpression and activation of these genes were associated with resistance to Dox and suggested a poor prognosis for patients.[29] In particular, researchers have indicated that the subunit of NADPH oxidase Rac1 contributes to Dox-induced cardiotoxicity via a ROS-dependent pathway and ROS-independent HDAC/p53 signaling.[30] And the activation of α7nAChR could decrease the expression of NOX2 and have a therapeutic potential against cardiovascular disease, which is consistent with our study.[31] These findings likely involve the demonstration that tVNS could improve Dox-induced oxidative stress, leading to the protection and repairment of cardiac structure and function.

In the current study, we also investigated the antitumor effect of tVNS. In recent years, a growing body of evidence suggested that targeting the neurological indicators of autonomic nerve innervation may offer a potential therapeutic strategy for intervening in tumor development and progression.[32] Sympathetic or parasympathetic nerves serve as positive or negative regulators vary among different cancer types.[8,33,34] Of which, either pharmacological or genetic blockade of sympathetic nerve and stimulation of parasympathetic fibers could improve the prognosis of breast cancer.[8] Our results indicated that the tVNS stimulation could reduce tumor growth and metastases. Several hypotheses explaining the prevention of progression and development of tumor growth exist. First, as the well-known anti-inflammation properties mediated through α7nAChR, tVNS could change the nature of the immune response from inflammatory to cytotoxic, thereby promoting the tumor cell apoptosis and reducing the tissue metastases.[35,36] This could be supported by our results that tVNS increased the tumor infiltration of $CD45^+CD3^+$ cells, as well as upregulated INFγ and downregulated TGFβ expressions. In addition, tVNS manipulates the

local nerves innervating tumors, this may partially alter the intratumoral neural infiltration niches and suppress the tumor microenvironment.[34] However, a detailed exploration of the potential mechanism is needed.

This study highlights the potential of tVNS as a promising therapeutic strategy for addressing the challenges posed by Dox-induced cardiotoxicity in cancer patients. We investigated the effects of tVNS in a tumor-bearing model, revealing potential therapeutic benefits that have a significant impact on Dox-induced cardiotoxicity and may even enhance the effectiveness of conventional cancer therapies. Moreover, our study underscores the need for further investigation into the mechanisms underlying these effects and the potential use of tVNS as a complementary therapy for cancer patients. This dual strategy significantly improves the therapeutic effect on Dox-induced cardiotoxicity and tumorigenesis, making it a promising candidate for clinical transformations.

Limitations of the study

There are several limitations to our study. First, HRV was assessed under isoflurane anesthesia. Although anesthesia may affect the assessed parameters, any such effect would be consistent across all groups in the study. Second, we mainly focused on the effects of the classical cholinergic anti-inflammatory pathway mediated by α7nAChR, and slightly consider the effects of non-cholinergic receptors. In addition, the speculations regarding the mechanism of anti-tumor effects were based on limited evidence. Therefore, the underlying effects on the tumor microenvironment are still unclear and require further exploration.

STAR★METHODS

Detailed methods are provided in the online version of this paper and include the following:

- KEY RESOURCES TABLE
- RESOURCE AVAILABILITY
  - Lead contact
  - Materials availability
  - Data and code availability
- EXPERIMENTAL MODEL AND STUDY PARTICIPANT DETAILS
  - Animals and cells
- METHOD DETAILS
  - Experimental design
  - Tragus vagus nerve stimulation
  - Echocardiography
  - Heart rate variability (HRV) analysis
  - Bioluminescence imaging
  - Histological assessment
  - Immunohistochemistry and immunofluorescence analysis
  - Transmission electron microscopy (TEM)
  - Elisa assay
  - Quantitative reverse transcription polymerase chain reaction (qRT–PCR)
  - Flow cytometry
  - Transcriptome analysis
- QUANTIFICATION AND STATISTICAL ANALYSIS
  - Statistical analysis

SUPPLEMENTAL INFORMATION

Supplemental information can be found online at https://doi.org/10.1016/j.isci.2024.109163.

ACKNOWLEDGMENTS

This work was supported by the grants from National Natural Science Foundation of China (82241057, 82270532, 81970287, 82100530, 82200556, and 82203891), and Foundation for Innovative Research Groups of Natural Science Foundation of Hubei Province, China (2021CFA010).

AUTHOR CONTRIBUTIONS

M.X., F.G., and L.S.: experimental conduction, and writing; X.H., S.X., W.T., X.L., Y.W.: data analysis and interpretation; L.Z. and Y.W.: drafting the article or critically revising it for important intellectual content. L.Y., H.J., and X.Z.: conception, design, and supervision. All authors contributed to the article and approved the submitted version.

DECLARATION OF INTERESTS

The authors declare no competing interests.

Received: September 25, 2023
Revised: November 14, 2023
Accepted: February 5, 2024
Published: February 13, 2024

REFERENCES

1. Li, D., Yang, Y., Wang, S., He, X., Liu, M., Bai, B., Tian, C., Sun, R., Yu, T., and Chu, X. (2021). Role of acetylation in doxorubicin-induced cardiotoxicity. Redox Biol. *46*, 102089. https://doi.org/10.1016/j.redox.2021.102089.
2. Levis, B.E., Binkley, P.F., and Shapiro, C.L. (2017). Cardiotoxic effects of anthracycline-based therapy: what is the evidence and what are the potential harms? Lancet Oncol. *18*, e445–e456. https://doi.org/10.1016/S1470-2045(17)30535-1.
3. Carrasco, R., Castillo, R.L., Gormaz, J.G., Carrillo, M., and Thavendiranathan, P. (2021). Role of Oxidative Stress in the Mechanisms of Anthracycline-Induced Cardiotoxicity: Effects of Preventive Strategies. Oxid. Med. Cell. Longev. *2021*, 8863789. https://doi.org/10.1155/2021/8863789.
4. Lai, Y., Zhou, X., Guo, F., Jin, X., Meng, G., Zhou, L., Chen, H., Liu, Z., Yu, L., and Jiang, H. (2022). Non-invasive transcutaneous vagal nerve stimulation improves myocardial performance in doxorubicin-induced cardiotoxicity. Cardiovasc. Res. *118*, 1821–1834. https://doi.org/10.1093/cvr/cvab209.
5. Lakoski, S.G., Jones, L.W., Krone, R.J., Stein, P.K., and Scott, J.M. (2015). Autonomic dysfunction in early breast cancer: Incidence, clinical importance, and underlying mechanisms. Am. Heart J. *170*, 231–241. https://doi.org/10.1016/j.ahj.2015.05.014.
6. Kalay, N., Basar, E., Ozdogru, I., Er, O., Cetinkaya, Y., Dogan, A., Inanc, T., Oguzhan, A., Eryol, N.K., Topsakal, R., and Ergin, A. (2006). Protective effects of carvedilol against anthracycline-induced cardiomyopathy. J. Am. Coll. Cardiol. *48*, 2258–2262. https://doi.org/10.1016/j.jacc.2006.07.052.
7. Fradley, M.G., Beckie, T.M., Brown, S.A., Cheng, R.K., Dent, S.F., Nohria, A., Patton, K.K., Singh, J.P., and Olshansky, B. (2021). Recognition, Prevention, and Management of Arrhythmias and Autonomic Disorders in Cardio-Oncology: A Scientific Statement From the American Heart Association. Circulation *144*, e41–e55. https://doi.org/10.1161/CIR.0000000000000986.
8. Kamiya, A., Hayama, Y., Kato, S., Shimomura, A., Shimomura, T., Irie, K., Kaneko, R., Yanagawa, Y., Kobayashi, K., and Ochiya, T. (2019). Genetic manipulation of autonomic nerve fiber innervation and activity and its effect on breast cancer progression. Nat. Neurosci. *22*, 1289–1305. https://doi.org/10.1038/s41593-019-0430-3.
9. Xu, M., Xue, R.Q., Lu, Y., Yong, S.Y., Wu, Q., Cui, Y.L., Zuo, X.T., Yu, X.J., Zhao, M., and Zang, W.J. (2019). Choline ameliorates cardiac hypertrophy by regulating metabolic remodelling and UPRmt through SIRT3-AMPK pathway. Cardiovasc. Res. *115*, 530–545. https://doi.org/10.1093/cvr/cvy217.
10. Elkholey, K., Niewiadomska, M., Morris, L., Whyte, S., Houser, J., Humphrey, M.B., and Stavrakis, S. (2022). Transcutaneous Vagus Nerve Stimulation Ameliorates the Phenotype of Heart Failure With Preserved Ejection Fraction Through Its Anti-Inflammatory Effects. Circ Heart Fail *15*, e009288. https://doi.org/10.1161/CIRCHEARTFAILURE.122.009288.
11. Yarmohammadi, F., Karbasforooshan, H., Hayes, A.W., and Karimi, G. (2021). Inflammation suppression in doxorubicin-induced cardiotoxicity: natural compounds as therapeutic options. Naunyn. Schmiedebergs. Arch. Pharmacol. *394*, 2003–2011. https://doi.org/10.1007/s00210-021-02132-z.
12. Yu, L., Huang, B., Po, S.S., Tan, T., Wang, M., Zhou, L., Meng, G., Yuan, S., Zhou, X., Li, X., et al. (2017). Low-Level Tragus Stimulation for the Treatment of Ischemia and Reperfusion Injury in Patients With ST-Segment Elevation Myocardial Infarction: A Proof-of-Concept Study. JACC. Cardiovasc. Interv. *10*, 1511–1520. https://doi.org/10.1016/j.jcin.2017.04.036.
13. Hoover, D.B. (2017). Cholinergic modulation of the immune system presents new approaches for treating inflammation. Pharmacol. Ther. *179*, 1–16. https://doi.org/10.1016/j.pharmthera.2017.05.002.
14. Ulloa, L. (2005). The vagus nerve and the nicotinic anti-inflammatory pathway. Nat. Rev. Drug Discov. *4*, 673–684. https://doi.org/10.1038/nrd1797.
15. Zhao, J., Yu, L., Xue, X., Xu, Y., Huang, T., Xu, D., Wang, Z., Luo, L., and Wang, H. (2023). Diminished alpha7 nicotinic acetylcholine receptor (alpha7nAChR) rescues amyloid-beta induced atrial remodeling by oxi-CaMKII/MAPK/AP-1 axis-mediated mitochondrial oxidative stress. Redox Biol. *59*, 102594. https://doi.org/10.1016/j.redox.2022.102594.
16. Alhowail, A. (2020). Varenicline enhances the survival of doxorubicin-treated mice. Eur. Rev. Med. Pharmacol. Sci. *24*, 11350–11355. https://doi.org/10.26355/eurrev_202011_23626.
17. Prathumsap, N., Ongnok, B., Khuanjing, T., Arinno, A., Maneechote, C., Apaijai, N., Chunchai, T., Arunsak, B., Shinlapawittayatorn, K., Chattipakorn, S.C., and Chattipakorn, N. (2022). Acetylcholine receptor agonists provide cardioprotection in doxorubicin-induced cardiotoxicity via modulating muscarinic M2 and alpha7 nicotinic receptor expression. Transl. Res. *243*, 33–51. https://doi.org/10.1016/j.trsl.2021.12.005.
18. Guo, F., Wang, Y., Wang, J., Liu, Z., Lai, Y., Zhou, Z., Liu, Z., Zhou, Y., Xu, X., Li, Z., et al. (2022). Choline Protects the Heart from Doxorubicin-Induced Cardiotoxicity through Vagal Activation and Nrf2/HO-1 Pathway. Oxid. Med. Cell. Longev. *2022*, 4740931. https://doi.org/10.1155/2022/4740931.
19. Curtiss, L.K., Black, A.S., Bonnet, D.J., and Tobias, P.S. (2012). Atherosclerosis induced by endogenous and exogenous toll-like receptor (TLR)1 or TLR6 agonists. J. Lipid Res. *53*, 2126–2132. https://doi.org/10.1194/jlr.M028431.
20. Herman, F.J., and Pasinetti, G.M. (2018). Principles of inflammasome priming and inhibition: Implications for psychiatric disorders. Brain Behav. Immun. *73*, 66–84. https://doi.org/10.1016/j.bbi.2018.06.010.
21. He, W.T., Wan, H., Hu, L., Chen, P., Wang, X., Huang, Z., Yang, Z.H., Zhong, C.Q., and Han, J. (2015). Gasdermin D is an executor of pyroptosis and required for interleukin-1 beta secretion. Cell Res. *25*, 1285–1298. https://doi.org/10.1038/cr.2015.139.
22. Fang, J., Wang, J., Chen, F., Xu, Y., Zhang, H., and Wang, Y. (2019). alpha7nAChR Deletion Aggravates Myocardial Infarction and Enhances Systemic Inflammatory Reaction via mTOR-Signaling-Related Autophagy. Inflammation *42*, 1190–1202. https://doi.org/10.1007/s10753-019-00979-2.
23. Lu, B., Kwan, K., Levine, Y.A., Olofsson, P.S., Yang, H., Li, J., Joshi, S., Wang, H., Andersson, U., Chavan, S.S., and Tracey, K.J. (2014). alpha7 nicotinic acetylcholine receptor signaling inhibits inflammasome activation by preventing mitochondrial DNA release. Mol. Med. *20*, 350–358. https://doi.org/10.2119/molmed.2013.00117.
24. Nocella, C., D'Amico, A., Cammisotto, V., Bartimoccia, S., Castellani, V., Loffredo, L., Marini, L., Ferrara, G., Testa, M., Motta, G., et al. (2023). Structure, Activation, and Regulation of NOX2: At the Crossroad between the Innate Immunity and Oxidative Stress-Mediated Pathologies. Antioxidants *12*, 429. https://doi.org/10.3390/antiox12020429.
25. Priya, L.B., Baskaran, R., Huang, C.Y., and Padma, V.V. (2017). Neferine ameliorates cardiomyoblast apoptosis induced by doxorubicin: possible role in modulating NADPH oxidase/ROS-mediated NFkappaB redox signaling cascade. Sci. Rep. *7*, 12283. https://doi.org/10.1038/s41598-017-12060-9.
26. Kyrychenko, S., Kyrychenko, V., Badr, M.A., Ikeda, Y., Sadoshima, J., and Shirokova, N. (2015). Pivotal role of miR-448 in the development of ROS-induced cardiomyopathy. Cardiovasc. Res. *108*, 324–334. https://doi.org/10.1093/cvr/cvv238.
27. Paravicini, T.M., and Touyz, R.M. (2008). NADPH oxidases, reactive oxygen species, and hypertension: clinical implications and therapeutic possibilities. Diabetes Care *31* (*Suppl 2*), S170–S180. https://doi.org/10.2337/dc08-s247.
28. Bedard, K., and Krause, K.H. (2007). The NOX family of ROS-generating NADPH oxidases: physiology and pathophysiology. Physiol. Rev. *87*, 245–313. https://doi.org/10.1152/physrev.00044.2005.

29. Paolillo, R., Boulanger, M., Gâtel, P., Gabellier, L., De Toledo, M., Tempé, D., Hallal, R., Akl, D., Moreaux, J., Baik, H., et al. (2022). The NADPH oxidase NOX2 is a marker of adverse prognosis involved in chemoresistance of acute myeloid leukemias. Haematologica *107*, 2562–2575. https://doi.org/10.3324/haematol.2021.279889.
30. Ma, J., Wang, Y., Zheng, D., Wei, M., Xu, H., and Peng, T. (2013). Rac1 signalling mediates doxorubicin-induced cardiotoxicity through both reactive oxygen species-dependent and -independent pathways. Cardiovasc. Res. *97*, 77–87. https://doi.org/10.1093/cvr/cvs309.
31. Hashimoto, T., Ichiki, T., Watanabe, A., Hurt-Camejo, E., Michaelsson, E., Ikeda, J., Inoue, E., Matsuura, H., Tokunou, T., Kitamoto, S., and Sunagawa, K. (2014). Stimulation of alpha7 nicotinic acetylcholine receptor by AR-R17779 suppresses atherosclerosis and aortic aneurysm formation in apolipoprotein E-deficient mice. Vascul. Pharmacol. *61*, 49–55. https://doi.org/10.1016/j.vph.2014.03.006.
32. Kamiya, A., Hiyama, T., Fujimura, A., and Yoshikawa, S. (2021). Sympathetic and parasympathetic innervation in cancer: therapeutic implications. Clin. Auton. Res. *31*, 165–178. https://doi.org/10.1007/s10286-020-00724-y.
33. Asnani, A., Moslehi, J.J., Adhikari, B.B., Baik, A.H., Beyer, A.M., de Boer, R.A., Ghigo, A., Grumbach, I.M., Jain, S., and Zhu, H.; American Heart Association Council on Basic Cardiovascular Sciences; Cardio-Oncology Science Subcommittee of Council on Genomic and Precision Medicine and Council on Clinical Cardiology; Council on Peripheral Vascular Disease; and Council on Arteriosclerosis, Thrombosis and Vascular Biology (2021). Preclinical Models of Cancer Therapy-Associated Cardiovascular Toxicity: A Scientific Statement From the American Heart Association. Circ. Res. *129*, e21–e34. https://doi.org/10.1161/RES.0000000000000473.
34. Silverman, D.A., Martinez, V.K., Dougherty, P.M., Myers, J.N., Calin, G.A., and Amit, M. (2021). Cancer-Associated Neurogenesis and Nerve-Cancer Cross-talk. Cancer Res. *81*, 1431–1440. https://doi.org/10.1158/0008-5472.CAN-20-2793.
35. Erin, N., Akdas Barkan, G., Harms, J.F., and Clawson, G.A. (2008). Vagotomy enhances experimental metastases of 4THMpc breast cancer cells and alters substance P level. Regul. Pept. *151*, 35–42. https://doi.org/10.1016/j.regpep.2008.03.012.
36. Erin, N., Barkan, G.A., and Clawson, G.A. (2013). Vagus nerve regulates breast cancer metastasis to the adrenal gland. Anticancer Res. *33*, 3675–3682.
37. Oh, J., Lee, B.S., Lim, G., Lim, H., Lee, C.J., Park, S., Lee, S.H., Chung, J.H., and Kang, S.M. (2020). Atorvastatin protects cardiomyocyte from doxorubicin toxicity by modulating survivin expression through FOXO1 inhibition. J. Mol. Cell. Cardiol. *138*, 244–255. https://doi.org/10.1016/j.yjmcc.2019.12.007.
38. Zhang, Y., Zheng, L., Deng, H., Feng, D., Hu, S., Zhu, L., Xu, W., Zhou, W., Wang, Y., Min, K., et al. (2022). Electroacupuncture Alleviates LPS-Induced ARDS Through alpha7 Nicotinic Acetylcholine Receptor-Mediated Inhibition of Ferroptosis. Front. Immunol. *13*, 832432. https://doi.org/10.3389/fimmu.2022.832432.

STAR★METHODS

KEY RESOURCES TABLE

REAGENT or RESOURCE	SOURCE	IDENTIFIER
Antibodies		
Tyrosine hydroxylase (TH)	Servicebio	Cat# GB11181; RRID: AB_2921651
Vesicular acetylcholine transporter (VACHT)	Abcam	Cat# ab235201
Neurofilament-L (NF-L)	Cell Signaling Technology	Cat# 2835; RRID: AB_490808
Zoombie NIRTM Fixable Viability Kit	Biolegend	Cat# 423105
CD16/32	Biolegend	Cat# 101319; RRID: AB_1574975
PE/Cyanine7 CD45	Biolegend	Cat# 103114; RRID: AB_312979
FITC CD3	Biolegend	Cat# 100203; RRID: AB_312660
Chemicals, peptides, and recombinant proteins		
Doxorubicin (Dox)	MCE	Cat# HY-15142
methyllycaconitine citrate	MCE	Cat# HY-N2332A
Critical commercial assays		
Creatine Kinase MB Isoenzyme Elisa assay kits	Ousaid Biotechnology Co., Ltd.	Cat# OSD-M0302
Cardiac Troponin T Elisa assay kits	Ousaid Biotechnology Co., Ltd.	Cat# OSD-M6102
Acetylcholine Elisa assay kits	Ousaid Biotechnology Co., Ltd.	Cat# OSD-M3001
Norepinephrine Elisa assay kits	Ousaid Biotechnology Co., Ltd.	Cat# OSD-M1346
Experimental models: Cell lines		
4T1-luc	ICell Bioscience Inc.	Cat#: iCell-m068
Experimental models: Organisms/strains		
Mouse: BALB/c (female)	the Animal Experimental Centre of Renmin Hospital of Wuhan University	N/A
Deposited data		
Transcriptomic data	This paper	SRA: PRJNA1064430 GEO: GSE2539599
Oligonucleotides		
Ncf1	TTCTTCAAAGTGCGGCCTGAT	CAGCTACGTTATTCTTGCCATCT
Ncf2	GGAGAAGTACGACCTTGCTATCA	ACAGGCAAACAGCTTGAACTG
Ncf4	GTCATCGAGGTCAAAACAAAAGG	TCCGAGTCTCAGCGATCTCTT
Rac2	GACAGTAAGCCGGTGAACCTG	CTGACTAGCGAGAAGCAGATG
Ccr1	CTCATGCAGCATAGGAGGCTT	ACATGGCATCACCAAAAATCCA
Cxcr2	TGTCTGGGCTGCATCTAAAGT	AGGTAACCTCCTTCACGTATGAG
Nlrp3	ATCAACAGGCGAGACCTCTG	GTCCTCCTGGCATACCATAGA
NPPA(ANP)	CACAGATCTGATGGATTTCAAGA	CCTCATCTTCTACCGGCATC
NPPB (BNP)	GTCAGTCGTTTGGGCTGTAAC	AGACCCAGGCAGAGTCAGAA
Software and algorithms		
CytoFLEX	Beckman Coulter, United States	N/A
R version 4.1	N/A	https://www.r-project.org/
Prism version 9.4.1	GraphPad Software	https://www.graphpad.com/features
Other		
Tragus vagus nerve stimulation device	Jinjiang, Chengdu, China	Cat#: S20

RESOURCE AVAILABILITY

Lead contact

Information and requests for resources and reagents should be directed to the Lead Contact, Dr. lilei Yu (lileiyu@whu.edu.cn).

Materials availability

This study did not generate new unique reagents.

Data and code availability

- The transcriptomic data have been deposited at GEO and SRA, and are publicly available. Accession numbers are listed in the key resources table. All data reported in this paper will be shared by the lead contact upon request.
- This paper does not report original code.
- Any additional information required to reanalyze the data reported in this paper is available from the lead contact upon request.

EXPERIMENTAL MODEL AND STUDY PARTICIPANT DETAILS

Animals and cells

Female BALB/c mice (6-8 weeks old) were obtained from the Animal Experimental Centre of Renmin Hospital of Wuhan University. The experimental procedures were in accordance with the Guideline for the Care and Use of Laboratory Animals outlined by the National Institutes of Health and approved by the Welfare & Ethics Committee of Renmin Hospital of Wuhan University (IACUC issue No. WDRM20220602B).

The 4T1 breast cancer cells transfected with luciferase (4T1-luc) were obtained from ICell Bioscience Inc. The cells were cultivated in RPMI-1640 supplemented with 10% fetal bovine serum (FBS) and 1% penicillin-streptomycin (Procell Life Science & Technology Co., Ltd) at 37°C and 5% CO2 in an incubator.

METHOD DETAILS

Experimental design

A total of 5×10^5 4T1-luc tumor cells were suspended in 100 μL phosphate-buffered saline and were then injected into the right fourth mammary fat pad of mice. The tumor volume was calculated with the following formula: $V = (L \times W^2) / 2$, where V indicated volume, and L and W represented length and width of the tumor, respectively, which was measured by a Vernier caliper once a week for 5 weeks. When the tumor volume reached at least 50 mm^3, mice were randomly distributed to the following 5 groups: (1) Control: 0.9% NaCl + sham tVNS; (2) tVNS: 0.9% NaCl + tVNS; (3) Dox: Dox + sham tVNS; (4) Dox + tVNS; (5) MLA: Dox + tVNS + methyllycaconitine citrate (MLA). Dox (HY-15142, MCE) was given at a cumulative dose of 20mg/kg via four weeks intraperitoneal (i.p) injections at 7, 14, 21, 28 d, and tVNS and MLA (HY-N2332A, MCE) (5mg/kg/day, i.p) were applied for 4 weeks from the first Dox dose.[37,38]

Tragus vagus nerve stimulation

tVNS was delivered through an electrical nerve stimulation device (S20, Jinjiang, Chengdu, China) as previously used.[7] The 20-Hz frequency and 1-mA amplitude were chosen as optimal for mice, which were within a safe range that was below the 10% of HR decreasing. For the sham tVNS procedure, the mice received the same procedure without electrical stimulation. During the active stimulation, tVNS caused in a modest decrease in heart rate, which did not result any adverse reactions yet increase vagal efferent activity.[20] In particular, the tVNS procedure (frequency 20 Hz, amplitude 1 mA, pulse width 1 ms) with the duty cycle of 1 s on and 1 s off was conducted to the bilateral tragus in the external auditory for 30 min per day under 1.5% isoflurane anesthesia up to 4 weeks after the first injection of Dox.

Echocardiography

Ultrahigh-resolution echocardiography was applied to evaluate cardiac function at 4 weeks after the initial Dox injection. Mice were anaesthetized with 1% isoflurane inhalation and maintained normal body temperature placed on a heated table. Echocardiographic parameters were measured under the long-axis view using a High-Resolution Imaging System (GE Vivid E95, USA).

Heart rate variability (HRV) analysis

Autonomic tone was assessed via the electrocardiogram (ECG) indices of HRV. Five-minute ECG recordings at lead II were performed once a week by the PowerLab data acquisition system (AD Instruments, New South Wales, Australia). The Frequency-domain (low frequency, 0.15 -1.5 Hz; high frequency, 1.5 -5 Hz) was analyzed by LabChart software (version 8.0, AD Instruments).

Bioluminescence imaging

At the endpoint of the experiment, the tumor-bearing mice were injected with 200 μL of D-Luciferin sodium (HY-12591, MCE) and anesthetized with 1% isoflurane in an induction chamber. Twenty minutes later, the mice were placed into an IVIS imaging system (IVIS Lumina LT

Series III, PerkinElmer) for imaging. Before the images were exported, the luminescence intensity scale was adjusted to the same range and the total photons were automatically counted using Living Image software (PerkinElmer).

Histological assessment

To estimate the extent of inflammatory filtration, and myocardial fibrosis, hematoxylin and eosin (H&E) and Masson's trichrome staining were conducted. Terminal deoxynucleotidyl transferase- mediated dUTP nick and labelling (TUNEL) staining was performed to access cardiac and tumor apoptosis. 4′,6-diamidino-2-phenylindole (DAPI; Thermo Fisher Scientific) was used to stain nucleic acids. All the tissue sections were analyzed by image analysis software (Image-Pro plus 6.0 imaging software, Media Cybernetics, Silver Spring, MD, USA) in a blinded manner.

Immunohistochemistry and immunofluorescence analysis

After euthanized with cervical dislocation, heart tissues were extracted from mice and fixed in 4% paraformaldehyde. Subsequently, the samples were processed and embedded in paraffin. The tissues were cut into 5μm tissue and prepared for further pathological examination. To evaluate the autonomic tone of heart tissues, the tyrosine hydroxylase (TH) was analyzed in the heart slides via immunohistochemistry. For immunofluorescence analysis, the sections were blocked with goat serum for 45 min and then incubated with rabbit polyclonal anti-VChAT antibody (ab235201, Abcam) and mouse monoclonal NF-L (Neurofilament-L) antibody (2835, Cell Signaling Technology). After incubation at 4°C overnight, the slices were washed three times with PBS and stained with goat anti-rabbit Alexa Fluor cy3 (111-545-003, Jackson) and goat anti-mouse Alexa Fluor 488 (111-165-003, Jackson) secondary antibodies. The slides were observed by Upright Fluorescent Microscope (EclipsE, Nikon) equipped with a digital camera (DS-U3, Nikon) and measured by Image-Pro plus 6.0 imaging software (Media Cybernetics, Silver Spring, MD, USA) in a blinded manner.

Transmission electron microscopy (TEM)

After sacrificing the mice, the fresh hearts were promptly removed, cut into 1-mm^3 clumps, and fixed in an electron microscope fixing solution (G1102, Servicebio) at 4°C for 2–4 h. Then, 1% Osmic acid in PBS was employed to post-fixed for 2h at room temperature and then was washed thrice. The samples were dehydrated using a density gradient of alcohol and embedded in SPI-Pon 812 epoxy resin (SPI, Cat#90529-77-4, PA, USA) overnight. Then the embedded tissues were polymerized for 48h at 60°C and cut into 60 -80nm ultrathin slices using a Leica UC7 ultramicrotome, which were further dyed and dried overnight at room temperature. The resultant slices were observed under an HT7700 transmission electron microscope (TECNAI G2 20 TWIN, FEI, USA).

Elisa assay

For the measurement of myocardial injury and autonomic activity, blood samples were collected via eyeball removal of each mouse. Serum was saved frozen at -80°C after centrifugating at 4500rpm, 4°C for 15 min. CK-MB (Creatine Kinase MB Isoenzyme), cTnT (Cardiac Troponin T), ACH (acetylcholine) and NE (norepinephrine) were detected using commercially available kits (OSD-M0302, OSD-M6102, OSD-M3001, OSD-M1346, Ousaid Biotechnology Co., Ltd.) following the manufacturer's instructions. The statistical software OriginPro 2021 (OriginLab, Northampton, MA, USA) was used to analyze the obtained data.

Quantitative reverse transcription polymerase chain reaction (qRT–PCR)

ANP, BNP, CXCR2, CCR1, NLRP3, NCF1, NCF2, NCF4, and RAC2 were detected in the cardiac tissues, and INFγ, TGFβ were evaluated in tumor tissue. GAPDH was for normalization. The relative gene expression levels were analyzed by $2^{-\Delta\Delta CT}$ method. Total RNA was extracted from left ventricular tissue and tumor tissue and then reverse transcribed by utilizing RevertAid First Strand cDNA Synthesis Kit (Thermo, K1622, USA). For qRT–PCR reactions, Fast Start Universal SYBR Green Master (Roche) and the 7500 real-time PCR system (Applied Biosystems, USA) were used to quantify the relative mRNA expression.

Flow cytometry

Tumor tissues dissected from tumor-bearing mice were processed to prepare cell suspensions. After incubation, the cells were analyzed via flow cytometry (CytoFLEX, Beckman Coulter, United States) and the data were further analyzed using FlowJo software. Briefly, the finely minced tissues were transferred to the digestion mix (0.15% Collagenase III, C8490, Solarbio) at 37°C for 2h, give it a good shake in every 15 min. The red blood cell lysis (R1010, Solarbio) the cell suspensions were added into cells suspensions to remove red blood cells. After filtration through a 70 μm nylon cell strainer, Cell suspensions were washed with sterilized PBS and incubated with the Zombie NIR™ fixable viability bit for 15 minutes at room temperature. Prior to surface staining, purified anti-mouse CD16/32 antibody (Biolegend, USA) was added to each sample to block nonspecific FcR binding. For staining of surface markers, the following antibodies were used at 4°C for 30 minutes: PE/Cyanine7 CD45 and FITC CD3. All these antibodies were purchased from Biolegend. After incubation, cells were analyzed using flow cytometry (CytoFLEX, Beckman Coulter, United States) and Data were further analyzed using FlowJo software.

Transcriptome analysis

Left ventricular myocardium from each group were utilized for RNA-Sequencing studies. For RNA-Sequencing studies, left ventricular myocardium from each group were excised quickly and snap-frozen in liquid nitrogen for further analysis. Total RNA was extracted using TRIzol

reagent and purified with the RNeasy Mini Kit and reversely transcripted into cDNA, according to the manufacturer's instructions. After quality control for raw data, SOAPnuke (v1.5.2, parameters: -l 5 -q 0.5 -n 0.1, BGI-Shenzhen, Shenzhen, China) was used to get clear read. The RNA sequencing data were aligned to the reference genomes using the HISAT (Hierarchical Indexing for Sliced Alignment of Transcripts, V2.0.4). Expression values were calculated as FPKM and differential genes were filtered with a 1.5-fold change cutoff and false discovery rate <0.05. Principal component analysis was performed to access sample clusters among groups. R software was used for hierarchical clustering analysis, Kyoto Encyclopaedia of Genes and Genomes (KEGG) pathway analysis and Gene Ontology enrichment of differentially expressed genes (DEGs) between different groups.

QUANTIFICATION AND STATISTICAL ANALYSIS

Statistical analysis

Data are presented as the mean ± SD. The normality of data distribution was tested using the Kolmogorov-Smirnov test. Kruskal-Wallis test was used when the group data were not normally distributed. Continuous data with normal distribution were analyzed by one-way ANOVA followed by Tukey's multiple-comparisons test. Differences with P values less than 0.05 were considered statistically significant. GraphPad Prism software 7.0 (GraphPad Software, Inc., La Jolla, CA, USA) and R software were used to conduct the statistical analyses.